

Connector Type-Controlled Mesophase Structures in Poly(propyl ether imine) Dendritic Liquid Crystals of Identical Dendrimer Generations

Prabhat Kumar,¹ D. S. Shankar Rao,² S. K. Prasad,² N. Jayaraman ¹

¹Department of Organic Chemistry, Indian Institute of Science, Bangalore 560012, Karnataka, India

²Centre for Nano and Soft Matter Sciences, Jalahalli, Bangalore 560013, Karnataka, India

Correspondence to: N. Jayaraman (E-mail: jayaraman@orgchem.iisc.ernet.in) or S. K. Prasad (E-mail: skpras@gmail.com)

Received 28 February 2017; accepted 21 June 2017; published online 00 Month 2017

DOI: 10.1002/pola.28709

ABSTRACT: Poly(propyl ether imine) (PETIM) dendrimers of one to three generations are used as dendritic cores to identify the influence of varying connector types that connect the dendritic core with peripheral mesogens on the emerging liquid crystalline (LC) properties. The LC properties vary in these dendritic liquid crystals, even when the dendrimer generations and thus the number of peripheral mesogenic moieties remain identical. PETIM dendrimer generations one to three, ester and amide connectors varying with succinates, phthalates, and succinamides, are studied herein. Cholesteryl moieties are installed at the peripheries through the above connectors to induce mesogenic properties. These modified dendritic liquid crystals reveal a layered mesophase structure in most ester and amide connector-derivatives, whereas a third-generation phthalate ester dendrimer favors a rectangular columnar mesophase

structure. A transition from layered to a rectangular columnar structure results by a mere change in the connector varying between a succinate or succinamide or phthalate, within one particular dendrimer generation and without altering the underlying dendrimer core or the number of mesogenic moieties. The study demonstrates that in dendritic liquid crystals with essentially identical chemical constitutions, a change in the connector type connecting the mesogen with the dendrimer core is sufficient to change the mesophase structures. © 2017 Wiley Periodicals, Inc. *J. Polym. Sci., Part A: Polym. Chem.* **2017**, *00*, 000–000

KEYWORDS: dendrimers; differential scanning calorimetry (DSC); glass transition; liquid crystals; X-ray

INTRODUCTION Fine structural features of a monomer building block govern the order and complexity of nanostructures.¹ Early pioneering work of Kunitake and Percec demonstrates that order and complexity, such as, one dimensional lamellae, two dimensional columns and three dimensional cubes can be modeled by appropriate designs of the basic structural blocks and attendant noncovalent interactions.^{2,3} In this context, nanophase segregation of distinct segments within the molecules⁴ having dendritic structural features hold a promise.^{5–11} Studies of the order and complexity, leading to distinct mesophase structures, were studied systematically using preformed dendrimers by modifying the peripheries with chosen mesogenic moieties.^{12–23} Elegant examples are (i) amphiphilic ionic second generation poly(amido amine) (PAMAM) dendrimer functionalized with differing amounts of myristic acid that exhibit a smectic A mesophase¹²; (ii) second-generation poly(propyleneimine) dendrimers peripherally functionalized with 4-methoxybiphenyl, 4-methoxyphenyl benzoate, *trans*-4-(4-pentylcyclohexyl)phenyl, 4-fluorobiphenyl, and 3,4,5-trifluorobiphenyl that exhibit a spontaneous homeotropic arrangement¹⁵ and (iii) azobenzene-

functionalized carbosilane dendrimers of first to fourth generations that prefers a smectic layer arrangement, whereas the fifth generation dendrimer of the same series prefers a rectangular columnar arrangement.¹⁶

In dendritic liquid crystals, dendritic cores are isotropic in nature. However, functionalization of the peripheries with anisotropic mesogenic moieties results in the formation of a mesophase. In all instances so far, it is seen that the mesophase structural arrangement changes as dendrimer generations and consequently the underlying dendritic molecular structures change drastically. For example, carbosilane dendrimers functionalized fully with alkyloxyazo derivative or butoxyphenylbenzoate exhibit a smectic A phase at zero to four generations, having 8, 16, 32, and 64 mesogenic moieties at their peripheries, respectively. However, the fifth generation dendrimer having 128 mesogenic moieties at the periphery shows a rectangular columnar mesophase.²² This change in the mesophase arrangement was accounted for by a dense packing of peripheral mesogenic moieties at the fifth generation. On the other hand, a lamellar arrangement is

Additional Supporting Information may be found in the online version of this article.

© 2017 Wiley Periodicals, Inc.

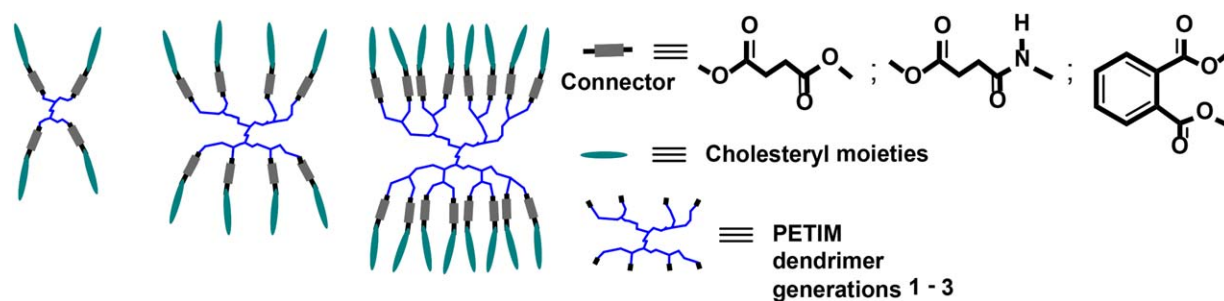


FIGURE 1 PETIM dendrimer cores having cholesteryl moieties at their peripheries through succinate, succinamide, and phthalate connectors connecting the peripheries with the core moiety. [Color figure can be viewed at wileyonlinelibrary.com]

preferred by decanoic, tetradecanoic, and octadecanoic acids-functionalized PAMAM dendrimer based mesogens, even for a higher generation dendrimer appended with 128 peripheral mesogenic units. Whereas when an altered dendrimer, namely, poly(propylene imine) (PPI) that possess shorter linker lengths between the branch points within the dendritic structure was used, a columnar arrangement in the mesophase was observed when periphery is functionalized with 64 mesogenic units only.²³

Important studies in dendritic liquid crystals to understand various aspects of mesophase evolution include: (i) changes in the dendrimer types, such as, carbosilane,²⁴ PAMAM,¹² PPI,^{13,15} and siloxane,¹⁶ and a homologous series of poly(propyl ether imine) (PETIM)¹⁹ dendrimers and changes in the dendrimer generations;²⁵ (ii) varying linker lengths connecting the dendrimer backbone and the mesogenic moiety;²⁶ (iii) varying alkyl chain length at the peripheries;²⁷ (iv) the mode of attachment of the mesogenic moiety to the dendrimer, such as, side on or end on;²⁸ (v) changing the shape of mesogenic moieties, such as, linear, radial and banana shaped²⁹ and the degree of branching in the core.³⁰ In the studies of dendritic LCs, to the best of our knowledge, no work has been reported so far which deals with the study of change in the mesophase by varying the flexibility and shape of the linkers within one particular dendrimer generation.

Changes in dendrimer generations and changes in the underlying dendrimer core structures lead to differing mesophase structures. Recently, we undertook an effort to verify as to how the mesophase structures would differ when a particular dendrimer generation is changed only with respect to the alkyl chains constituting the dendrimer core structure alone, without changing the branching pattern and the number of mesogenic moieties.¹⁹ Thus, when the *n*-propyl moieties connecting the branch points at the interior dendrimer structure were replaced with ethyl moieties, a distinct transition of the mesophase structure from one-dimensional smectic (SmA) to a columnar in-plane modulated smectic (modulated Sm \tilde{A}) structure emerged.

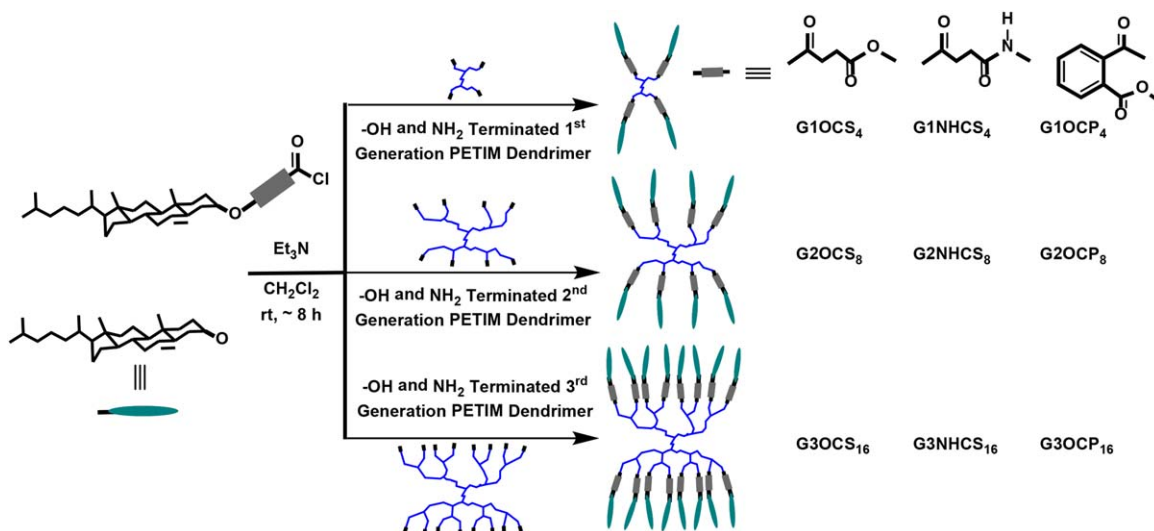
The studies warrant identifying the role of the functional group that act as connectors to connect the isotropic dendrimer core with the peripheral mesogenic segment in the

mesophase formation, specifically, without changing the chemical structure of the dendritic core. A systematic change in the rigidity and the nature of the connectors connecting the dendritic core with the mesogenic moieties is of central importance, to correlate the role of the nonmesogenic dendritic core and the attendant mesophase structures. In this effort, we report herein a study of the first, second and third generation PETIM dendrimers, functionalized with cholesteryl moieties through three different types of connectors, namely, succinate, phthalate, and succinamide (Fig. 1). As many as nine derivatives are synthesized within these three generations of dendrimers, having changes only in the connector type connecting the mesogenic peripheral segment with the dendritic core. A profound change in the mesophase structures occurs as a result of a change in the connector, even when the dendrimer core and peripheral mesogenic constituents are identical within each generation.

RESULTS AND DISCUSSION

Synthesis

Amine and hydroxyl groups terminated PETIM dendrimers up to three generations were used in the present study. These dendrimers were synthesized by a divergent growth method as established previously.³¹ To covalently attach the peripheries of these dendrimers, hydroxyl groups-terminated dendrimers were reacted with cholesterylhemisuccinoyl chloride or cholesterylhemiphthaloyl chloride, in the presence of Et₃N in chloroform at 0 °C for ~10 h, to afford the corresponding cholesteryl ester derivatives with succinate or phthalate connectors in good yields (Scheme 1). Similarly, amine-terminated PETIM dendrimers were reacted with cholesterylhemisuccinoyl chloride to secure dendrimers having succinamide connectors at their peripheries. The crude reaction mixtures were subjected to differential solubility in a solvent, so as to obtain the pure products. Thus, the crude reaction mixture was made suspension in *n*-hexane, stirred for ~15 min., centrifuged, hexane-solubilized portion collected, and solvent evaporated *in vacuo*. The resulting residue was subjected to treatment with *n*-hexane iteratively for few times, by which the products were isolated pure. The dendritic liquid crystals are glassy solids and soluble in hexane, toluene, dichloromethane, and chloroform and sparingly soluble in methanol, dioxane, and THF. Molecular structures



SCHEME 1 Synthesis of succinate, succinamide and phthalate ester connector type dendritic liquid crystals of generations 1 - 3. [Color figure can be viewed at wileyonlinelibrary.com]

of only the third generation dendritic liquid crystals are shown in Figure 2. The constitutions and structural homogeneities of all derivatives were characterized by spectroscopies and elemental analyses. In the FTIR spectrum, carbonyl stretching frequency was observed at $\sim 1732\text{ cm}^{-1}$, corresponding to the ester functionality. In ^1H NMR spectrum, methylene protons attached to peripheral hydroxyl group of dendrimers shifted from $\delta = 3.6$ to 4.1 ppm and appeared as a triplet, with a coupling constant of ~ 5.8 Hz, corresponding to CH_2OCO functionalities in succinate connected dendrimers. In ^{13}C NMR spectrum, appearance of resonance at ~ 170 ppm confirmed the ester functionality. Elemental composition analyses confirmed the homogeneity of the products. In the case of the amide series, IR spectrum showed disappearance of peak at 1704 cm^{-1} ($-\text{CO}_2\text{H}$) and appearance of peaks at ~ 1650 and

$\sim 1550\text{ cm}^{-1}$, corresponding to the amide bond stretching frequencies. The amide bond formation led to a downfield shift of $-\text{CH}_2\text{NH}_2$ moieties of un-functionalized dendrimers from 2.7 to 3.35 ppm, corresponding to the formation of CH_2NHCS linkage. Resonance at ~ 5.38 and ~ 3.35 ppm in ^1H NMR spectra corresponded to olefinic protons of cholesteryl moiety and $\text{NH}-\text{CH}_2-$ protons of the dendrimer scaffold, respectively. In ^{13}C NMR spectrum, resonance at ~ 170 ppm corresponded to carbonyl-moiety of the ester and amide functionalized dendrimers. Elemental analyses confirmed further the structural homogeneities of all the derivatives.

Mesophase Studies of Dendritic Liquid Crystals

Molecular masses of the dendritic liquid crystals range between 1070 and 11712 g mol^{-1} , representing molecular

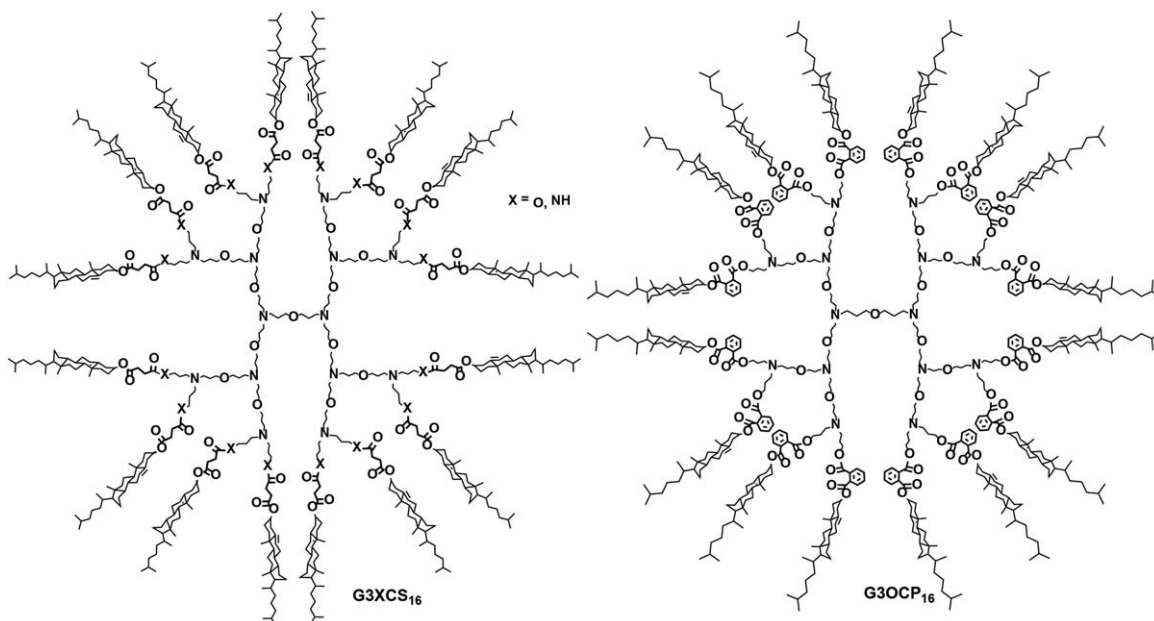


FIGURE 2 Molecular structures of G3OCS_{16} , G3NHCS_{16} , and G3OCP_{16} dendritic liquid crystals.

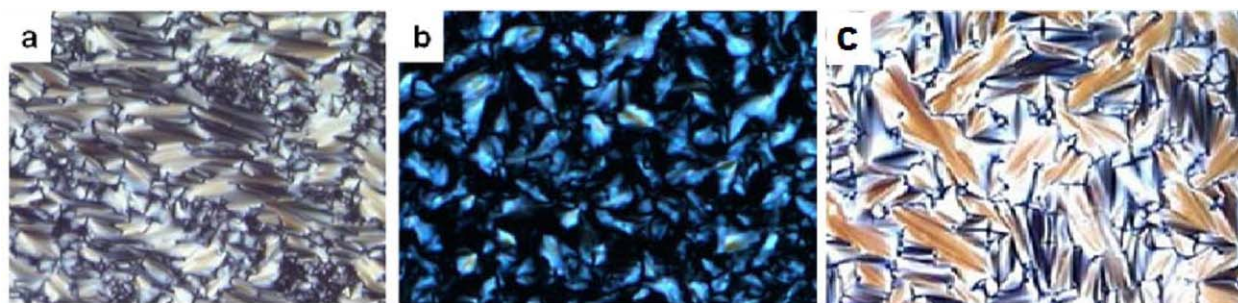


FIGURE 3 POM textures of (a) **G3OCS₁₆** at 82 °C; (b) **G3OCP₁₆** at 98 °C, and (c) **G3NHCS₁₆** at 90 °C in the cooling cycle. [Color figure can be viewed at wileyonlinelibrary.com]

masses of low molecular weight compounds to macromolecules. Even with such large gradations in the molecular masses, facile characterization of mesomorphic properties was possible on all the derivatives, through polarizing optical microscope (POM), differential scanning calorimeter (DSC), and powder X-ray diffraction (XRD) analyses.

Thermal characterization by POM reveals that functionalization of the dendrimer peripheries with cholesteryl moieties induces a mesomorphic behavior on all derivatives. An enantiotropic mesophase texture is observed with all derivatives in POM between room temperature and isotropic transition. The mesophase to isotropic transition temperature varied with each cholesteryl-phthalate dendritic mesogens, between 111 and 117 °C. The transition temperatures were: **G1OCP₄**, with 4 phthalates, melted at 110 °C and birefringence regained at 99 °C on cooling; **G2OCP₈**, with 8 phthalates, melted at 107 °C, retrieved birefringence at 96 °C; **G3OCP₁₆**, with 16 phthalates, showed clearing transition at 117 °C and mesophase reappeared at 108 °C in the cooling cycle. Subsequent heating-cooling cycles showed similar transitions and the phase transition temperatures were traced nearly the same. In the case of the amide connectors, first generation **G1NHCS₄** exhibited isotropic phase at 157 °C and upon cooling, a leaflet structure began to appear from 148 °C. Second generation **G2NHCS₈** exhibited an enantiotropic mesophase, which was recognised by characteristic bâtonnets, arising from the dark isotropic phase at 134 °C in the cooling cycle, which were fully grown to a fan-like texture. The homeotropic regions of the texture retained till room temperature. The transitions from isotropic to mesophase for **G3NHCS₁₆** at 150 °C were accompanied by the formation of focal conic, which was retained till room temperature. **G3OCS₁₆**, **G3OCP₁₆**, and **G3NHCS₁₆** showed a mesophase to isotropic transition occurred at 104, 117, and 161 °C, respectively, which upon cooling regained the texture (Fig. 3).

A complete extinction of the texture was observed when the analysis was performed on a substrate coated with a surfactant, which is a hallmark of the phase being non-tilted type.³² Important observations are that (i) the succinate connector series have lower glass transition and clearing temperatures than other two connectors series; (ii) the clearing temperatures of the amide connector series are higher and

(iii) the glass transition temperatures of the phthalate connector series are observed to be higher than remaining two series (Fig. 4). Within each connector series, both glass transition and clearing temperatures are not significantly different. Higher glass transition temperature in the case of phthalate connector series implies that aromatic linker shortens the mesophase temperature at the expense of the glass transition temperature, as opposed to the connectors being aliphatic in nature. The amide connector series exhibited higher clearing temperatures, implying a more rigid molecular structure.

Phase transitions were analyzed subsequently through DSC technique, with heating-cooling rate maintained at 10 °C min⁻¹, using hermetically sealed pans. Thermal data of all dendritic LCs are given in Table 1. Enantiotropic nature of the mesophase transitions was observed in the DSC analysis of the ester series dendrimers. The broad step transition near room temperature in the heating and cooling cycles and a shift in the base line prior-to and after the transition in all derivatives suggested a glass transition, rather than a crystallization transition. The succinic ester connector series showed glass transition temperature range between 18 and 24 °C, and isotropization temperature range between 100

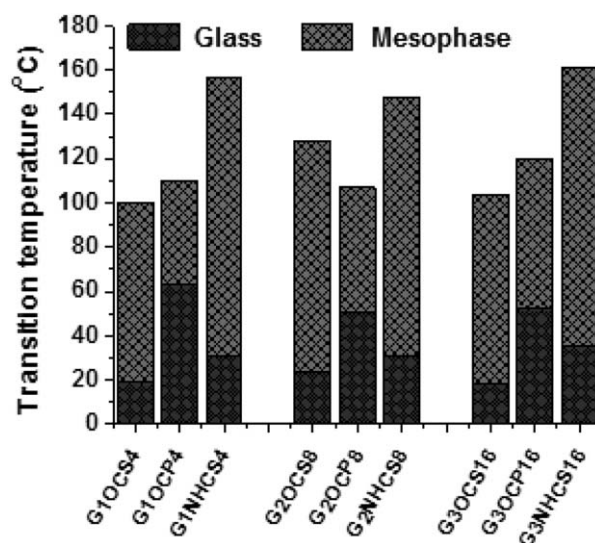


FIGURE 4 Phase transitions of dendritic liquid crystals.

TABLE 1 Thermal and Thermodynamic Data for the Phase Transitions Observed in Second Heating-Cooling Scan ($10\text{ }^{\circ}\text{C min}^{-1}$)

Compound [Mass (kDa)]	Transitions ^a ($^{\circ}\text{C}$), ΔH (kJ mol^{-1})
G1OCS₄ (2.239)	g 19 SmA 100 (5.0) 100 (5.4) SmA 18 g
G1NHCS₄ (2.468)	g 31 SmA 157 (10.4) 148 (9.2) SmA 26 g
G1OCP₄ (2.432)	g 63 SmA 110 (4.96) 99 (6.13) SmA 54 g
G2OCS₈ (4.807)	g 24 SmA 128 (7.7) 121 (8.5) SmA 12 g
G2NHCS₈ (5.264)	g 31 SmA 148 (17.9) 134 (16.8) SmA 23.5 g
G2OCP₈ (5.192)	g 51 SmA 107 (8.40) 96 (8.26) SmA 44 g
G3OCS₁₆ (9.943)	g 18 SmA 104 (30.40) 98 (28.8) SmA 17 g
G3NHCS₁₆ (10.856)	g 35 SmA 161 (25.2) 150 (25.4) SmA 27 g
G3OCP₁₆ (11.712)	g 54 Col _r 114 (16.60) 102 (16.71) Col _r 48 g

^a g, glass; Sm, smectic; I, isotropic.

and $128\text{ }^{\circ}\text{C}$. When comparing the role of connector moiety, the isotropization temperature for phthalate ester connector series were between 107 and $117\text{ }^{\circ}\text{C}$, whereas the glass transition temperature was observed between 51 and $63\text{ }^{\circ}\text{C}$ (Fig. 5). The glass and isotropization transition temperatures for the first generation derivative **G1OCP₄** were 63 at $110\text{ }^{\circ}\text{C}$, respectively, in the heating scan. Whereas, on cooling, these transitions were observed at 99 and $54\text{ }^{\circ}\text{C}$. Second generation **G2OCP₈** showed glass transition and mesophase to isotropic transition at 51 and $107\text{ }^{\circ}\text{C}$ in the heating scan, whereas the cooling scan showed these transitions at 96 and $44\text{ }^{\circ}\text{C}$. For third generation dendrimer **G3OCP₁₆**, glass transition and isotropization temperatures were 54 and $117\text{ }^{\circ}\text{C}$ in the heating scan, and cooling scan showed transitions at 108 and $48\text{ }^{\circ}\text{C}$, respectively. Phase transitions of succinate ester series **G1OCS₄** and **G2OCS₈** were observed between 19 and $128\text{ }^{\circ}\text{C}$. **G3OCS₁₆** showed glass transition and isotropization temperatures at 18 and $104\text{ }^{\circ}\text{C}$ in the heating cycle, respectively, whereas in the cooling scan, these transitions were found to be 99 and $17\text{ }^{\circ}\text{C}$, with a change in molar enthalpy (ΔH) per mesogenic unit of 1.9 kJ mol^{-1} .

In the amide connector series, first generation **G1NHCS₄** showed glass transition and isotropization temperatures at 31 and $157\text{ }^{\circ}\text{C}$ in the heating scan, whereas these transitions were observed at 148 and $26\text{ }^{\circ}\text{C}$ during cooling scan. Second

generation **G2NHCS₈** showed a narrower mesophase range, during heating scan, the glass transition and clearing transition temperatures were observed at 31 and $148\text{ }^{\circ}\text{C}$, whereas these transitions were observed at 134 and $24\text{ }^{\circ}\text{C}$ during cooling scan. The third generation **G3NHCS₁₆** showed transitions at 35 and $161\text{ }^{\circ}\text{C}$ during heating scan, whereas these were observed at 150 and $27\text{ }^{\circ}\text{C}$ during cooling scan. Further, change in molar enthalpy was found to be increasing across the generations and the change in molar enthalpy per mesogenic unit was found to be between 1.5 and 2.5 kJ mol^{-1} . ΔH values were seen to be progressively higher as the generations advance, indicating an increased molecular packing in the higher generations. Among the third generation dendrimers, a higher ΔH value of SmA to isotropic transition was observed for **G3OCS₁₆**, which might result from an altered molecular packing of this third generation, succinate connector derivative, when compared with amide and phthalate connected dendrimers. A general trend of dendrimer generations is that the prolate-shaped structures of lower generation become spheroidal in nature in higher generation dendrimers.³³ It is likely that this topological change among dendrimer generations causes the molecular packing different among the generations and the resulting molar enthalpy changes of phase transitions. The work of Serrano and coworkers shows a similar change in isotropization entropies and temperatures wherein the columnar mesophase

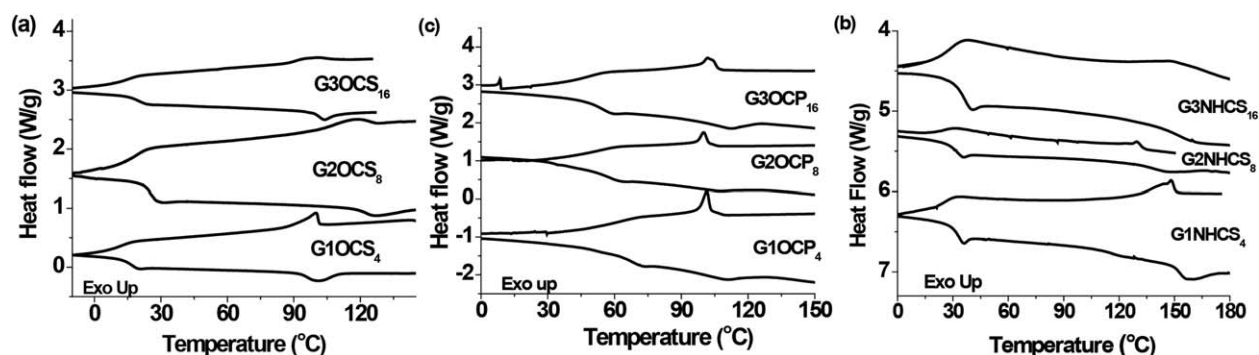


FIGURE 5 DSC thermograms of (a) ester-linked and (b) amide-linked PETIM dendritic liquid crystals (heating-cooling rate $10\text{ }^{\circ}\text{C min}^{-1}$, second cycle).

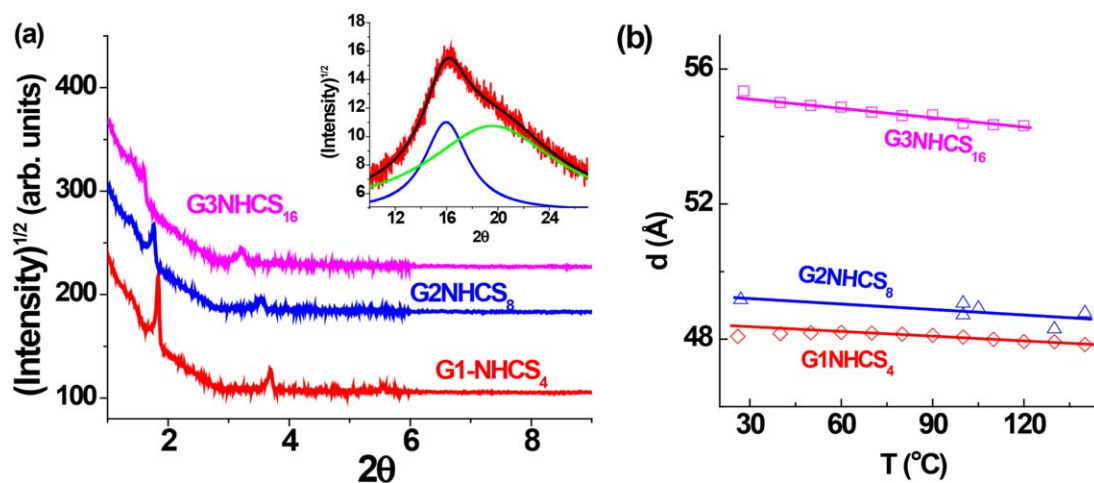


FIGURE 6 (a) XRD profile of amide-linked dendritic liquid crystals (Inset: Lorentzian fit for wide angle region) and (b) change in layer thickness with temperature. [Color figure can be viewed at wileyonlinelibrary.com]

has smaller isotropization entropy than that of lamellar mesophase. This effect was attributed to conformational changes within the molecules, originating from different segments of the codendrimer molecules.³⁴

XRD Study

Variable temperature XRD studies were conducted to enable the identification of the mesophase structures of all derivatives. For all the dendritic LCs, variable temperature XRD patterns, within the mesomorphic range, consisted of at least two sharp equidistant peaks in the low-angle region and a broad, diffuse maximum in the wide angle region (Figs. 6–8, Table 2). The ratio of the reciprocal of the spacings of low angle reflections, being integral numbers, indicated the presence of a lamellar arrangement in the mesophase for all the dendritic liquid crystals, except **G3OCP**₁₆. The broad, diffuse

halo suggested a short range, liquid-like order. A generation-dependent trend in the layer thickness was found in dendritic liquid crystals. Concerning the influence of generation and the type of linkage on the magnitude of the spacing, the layer thickness of the compounds were found to be increasing across the generations (Figs. 6 and 7). The layer thickness in both succinate and phthalate series decreased linearly with increasing temperature at principal and higher order reflections. Increasing temperatures thus shortened the molecular length marginally, possibly as a result of altered segmental balance between the relatively hydrophilic dendritic core region and lyophilic cholesteryl peripheral region. A weak but perceptible increase in one of the intermolecular distances also occurred with increasing temperature (Table 2). In addition to the trend of the larger spacing inferred from small angle diffraction pattern, the observed

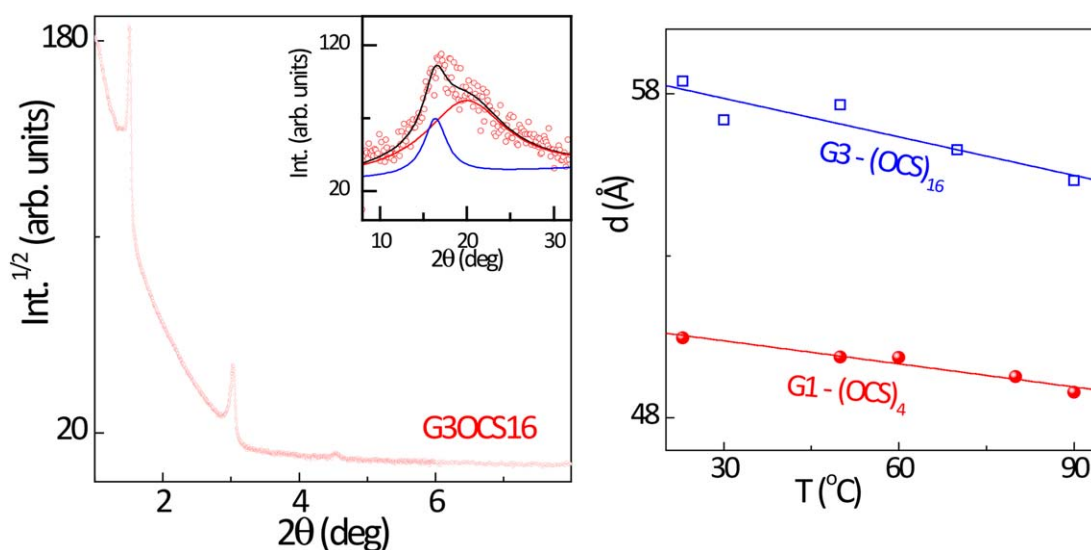


FIGURE 7 Left: XRD profile of **G3OCS**₁₆ at 23 °C bringing out the lamellar nature of the structure. Inset: Diffuse maximum in the wide angle region described by a sum (black line) of two Lorentzian functions with the resolved individual peaks depicted by blue and red lines. Right: Change in layer thickness with temperature. [Color figure can be viewed at wileyonlinelibrary.com]

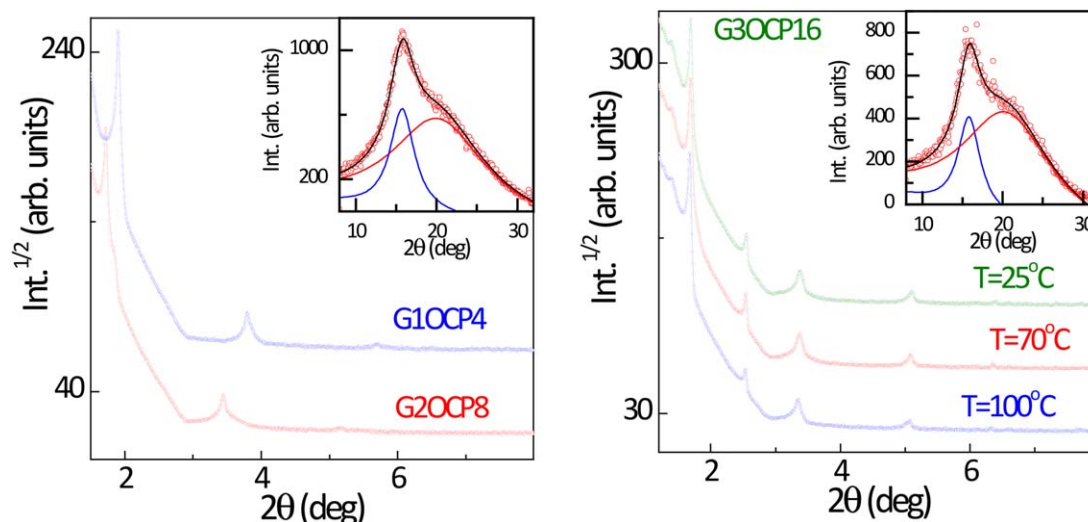


FIGURE 8 Small angle XRD profiles of **G1OCP₄** and **G2OCP₈** (left). The inset shows the wide angle maximum of **G2OCP₈** (black line) being described by two Lorentzians (blue and red lines). Variable temperature XRD profiles of **G3OCP₁₆**, presenting the increase of the lamellar spacing (lowering of Bragg angle) with decreasing temperature (right). (Inset: Diffraction in the wide angle region for **G3OCP₁₆**). [Color figure can be viewed at wileyonlinelibrary.com]

diffuse halo in the wide angle region corresponded to short range order. The wide angle profiles were fit into a sum of two Lorentzians, suggesting to the possibility of two types of packing within the layer. Two partially overlapping broad

peaks centered at about 5.5 and 4.5 Å (D_{w1} and D_{w2} in Table 2), with the former corresponding to the average distance between the cholesterol moieties and the latter arising from the flexible dendritic core.

TABLE 2 XRD Spacings Corresponding to the Layer Periodicity, Its Harmonics, and Intermolecular Distance (D) Within the Layer of Dendritic LCs

Compound	T (°C)	d_{100} (Å)	d_{200} (Å)	d_{300} (Å)	D_{w1} (Å)	D_{w2} (Å)	D_{w3} (Å)
G1OCS₄	23	50.46	25.19	16.79	5.4	4.5	
	60	49.87	24.90	16.6	5.5	4.6	
	90	48.79	24.35		5.5	4.5	
G1NHCS₄	26	48.08	23.95	15.93	5.59	4.58	
	150	48.34	23.94	15.90	5.70	4.47	
G1OCP₄	25	46.51	23.28	15.49	5.64	4.46	2.85
	60	46.61	23.32	15.53	5.66	4.44	2.85
	100	45.91	23.00	15.32	5.70	4.30	2.86
G2OCS₈	24	49.33	24.65		5.5	4.4	
	100	49.18	24.72		5.6	4.5	
	130	48.27	24.28				
G2NHCS₈	27	50.23	24.39	16.26	5.59	4.57	
	140	48.77	24.25		5.66	4.27	
G2OCP₈	26	51.09	25.65	17.12	5.62	4.40	2.85
	60	51.12	25.67	17.10	5.66	4.41	2.85
	100	50.63	25.32	16.88	5.68	4.31	2.86
G3OCS₁₆	23	58.39	29.15	19.44	5.41	4.46	
	50	57.66	28.78	19.14			
	90	55.32	27.61		5.48	4.56	
G3NHCS₁₆	28	55.35	27.51	18.29	5.51	4.50	
	120	54.32	27.06	17.93	5.65	4.62	

TABLE 3 XRD Spacings Corresponding to the Layer Periodicity, Its Harmonics, and Intermolecular Distance Within the Layer of G3OCP₁₆

25 °C			70 °C			100 °C					
d_{obs} (Å)	d_{calc} (Å)	hkl	Lattice parameter (Å): Col _r	d_{obs} (Å)	d_{calc} (Å)	hkl	Lattice parameter (Å): Col _r	d_{obs} (Å)	d_{calc} (Å)	hkl	Lattice parameter (Å): Col _r
52.13	52.13	010	$a = 46.3$	52.22	52.22	010	$a = 46.4$	52.66	52.66	010	$a = 46.6$
34.62	34.62	110	$b = 52.1$	34.69	34.69	110	$b = 52.2$	34.81	34.87	110	$b = 52.7$
26.16	26.06	020		26.18	26.11	020		26.36	26.33	020	
17.31	17.31	030		17.38	17.41	030		17.53	17.55	030	
13.81	13.90	040		13.90	13.92	230		5.80	5.81	190	

Presence of the second diffuse peak is more pronounced, which is assumed to be due to the increased number of cholesterol moieties present in higher generation dendritic LCs. A comparison between the two series of connectors shows interesting difference due to the linkers. Between **G1OCS₄** and **G1OCP₄**, the layer thickness reduced considerably in **G1OCP₄**. The phthalate connector thus rigidified the molecule more than the flexible succinate, even when in both the cases the diester moieties are separated by two carbons only. The intermolecular distance of 5.4 Å in **G1OCS₄** to 5.64 Å in **G1OCP₄** would correspond to the average distance between the cholesterol moieties. Whereas, the observed second intermolecular distance of 4.5 and 4.46 Å would correspond distance arising from the disordered dendritic backbone. These intermolecular distances did not change with linker variation. A third distance (D_{w3}) was observed in the phthalate series only, the origin of which is likely to be the inter-phthalate moiety distance within the molecule. Such a distance, measured from wide angle region, however, could not be identified in the case of the succinate connector series. A further point that may be noted from the temperature dependence of the lamellar spacing is that the succinate connector dendritic liquid crystals possessed a larger variation than the phthalate ester connector dendritic liquid crystals, possibly as a result of succinate connector being more flexible than phthalate ester system.

The layer thickness was compared with the length of a dendritic LCs, assuming that the dendrimer is prolate in shape, with the cholesterol units stretching out on both sides of the central dendrimer core. For this purpose, the diameter of dendrimers cores of 8, 15, and 22 Å were used, as evaluated by molecular dynamics simulations, for the G1, G2, and G3 dendrimers, respectively.³³ The length of one cholesterol unit is about 18 Å.³⁵ Combining with the connector lengths, the length of G1, G2, and G3 generation dendrimers are estimated to be ~ 56, 63, and 70 Å, respectively. The observed d_{100} values for all these dendritic LCs at room temperature are lower than the estimated molecular lengths. We premise that the difference between the observed spacings and the estimated molecular lengths is due to: (i) a shortening of

primary layer spacing owing to a layer formation constituted by each molecule without much interdigitation and the molecular compaction and/or (ii) tilting of the individual cholesterol units with respect to the dendrimer core segment, with a randomness in the tilting direction.

Variable temperature powder XRD pattern of **G3OCP₁₆** differed significantly from those of remaining dendritic liquid crystals studied herein. At 100 °C, five peaks were observed in small angle region, the qualitative pattern remaining the same at different temperatures (Fig. 8). Presence of multiple sharp peaks, with a nonintegral ratio between them, together with a diffuse maximum in the wide angle region and the plane group $P2mg$, suggests the formation of two-dimensional self-assembled noncentered rectangular columns. The multiple sharp peaks also suggest a two dimensional lattice. These features are also observed at other temperatures for which the scans are obtained. The relevant spacing and lattice parameters are listed in Table 3. A schematic representation of the molecular arrangements in the columnar mesophase is given in Figure 9.

The non-centered rectangular columnar mesophase³⁶ can be referred equivalently to the modulated smectic A phase, with the lattice directions one in the layer plane and another along the layer normal.³⁷ However, we find that the observed reflections consistent a rectangular columnar structure with a $P2mg$ symmetry. Comparing the layer thickness of the dendritic LCs, the lattice parameter of **G3OCP₁₆** along one of the axes is comparable to the layer thickness of the remaining third generation dendritic liquid crystals studied herein. The volume fractions of dendritic core versus the peripheral moieties is ~ 3% larger with succinate and amide connector derivatives, in comparison with phthalate connector derivatives, by which the accessible region for individual peripheral cholesterol moieties is marginally larger for **G1OCS₄**, **G2OCS₈**, **G3OCS₁₆**, **G1NHCS₄**, **G2NHCS₈**, and **G3NHCS₁₆** derivatives than for **G1OCP₄**, **G2OCP₈**, and **G3OCP₁₆** derivatives. The more pronounced effect for the third generation **G3OCP₁₆** to adopt a rectangular columnar mesophase structure, in comparison to third generation **G3OCS₁₆** and **G3NHCS₁₆** that adopt a lamellar structure, could be

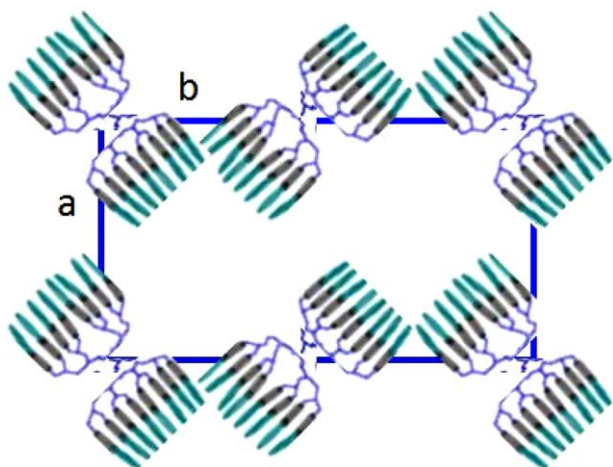


FIGURE 9 A representation of the molecular arrangement of the noncentered rectangular columnar structure with plane symmetry $P2mg$ exhibited by $G3OCP_{16}$ dendritic liquid crystal. [Color figure can be viewed at wileyonlinelibrary.com]

attributed to the presence of ortho-disubstituted phthalic moiety. We premise that changes in the globular structures among the three third generation dendrimers, varying only with respect to the nature of succinate, phthalate, and amide connectors, alter the mesophase structure, between a lamellar structure and a noncentered rectangular columnar structure.

The appearance of rectangular columnar phase has been observed commonly in many instances earlier. Few examples are (i) ionic liquid crystals derived from 3,4,5-trialkoxybenzyl trimethyl - benzenammonium cation with BF_4 and PF_6 counteranions;³⁸ (ii) dodecyl chains attached at the periphery of the aryl moiety at one imide position of a perylene diimide or naphthalenediimide core and triethyleneglycol chains at the periphery of the aryl moiety on the other side of the molecules;^{39,40} (iii) viologens possessing tri-alkoxy phenyl moiety at each terminal having dodecyl and hexadecyl chain;⁴¹ and (iv) liquid crystals derived from N,N' -bis(3,4,5-trialkoxyphenyl)ureas with octyl, dodecyl, and hexadecyl chains.⁴²

Rectangular columnar mesophase are shown by dendritic liquid crystals previously. For example, (a) a fourth generation amine-terminated PAMAM complexed with linear tetradecanoic acid;²³ (b) a third generation PAMAM dendrimer, functionalized with varying proportions of two types of promesogen moieties;^{34,43} (c) triazine-based dendrimers containing central linkers with odd numbers of carbon atoms and C3-symmetrical dendrimers with rigid core;⁴⁴ and (d) a carbosilane fifth generation dendrimer fully functionalized with alkyloxyazo derivative or butoxyphenylbenzoate derivative at its periphery.²² The effect was attributed to varying dendrimer generations, namely, lower-to-higher dendrimer generations and thus, a drastic structural change of the underlying dendritic core itself.

The effect of the dendrimer generations, the role of linkers or spacers connecting the dendritic core with the peripheral

moieties, presence of mono- to multiple mesogen-inducing segments at the peripheries, multiplicities of branching at the dendritic core and branch junctures were studied in detail for a long time. Frey and coworkers demonstrated in an early work that carbosilane dendrimers installed with 12, 36, and 108 perfluoroalkyl moieties of one to three generations exhibited generation dependent mesophase properties. Whereas the first generation dendrimer showed a layered phase, second and third generation dendrimers adopted a hexagonal columnar phase, due to high density of surface moieties and the lack of sufficient spacer length to decouple the perfluoroalkyl groups and the dendrimer core.⁴⁵

Meijer and coworkers demonstrated in a very early work that PPI dendrimers derivatized with 4, 16, and 64 pentyloxycyanobiphenyl and decyloxycyano-biphenyl moieties at the peripheries of first, second, and generation dendrimers, respectively, all exhibited a layered smectic phase only. A phase separation of dendritic core with distorted conformation and the peripheral cyanobiphenyl moiety oriented in an antiparallel arrangement, leading to an interdigitated bilayer structure, was suggested to rationalize the observations.⁴⁶ Similar smectic phase was observed in another series of PPI that were tethered with ω -(4'-cyanobiphenyloxy)alkyl substituted first and second generation dendritic liquid crystals by Yonetake and Ueda.⁴⁷

A fine balance of the linker length and densities of the peripheral moieties on the evolution of mesogenic properties was observed on dendrimers possessing triphenylene core and sugar-coated peripheries, that are connected through the alkylene linkers. A decyl-linker connecting the core with mono-sugar moiety at the periphery exhibited a rectangular columnar arrangement. Whereas, the same linker connecting the core with a tris-sugar moiety at the periphery led to hexagonal columnar mesophase structure.⁴⁸

Serrano and coworkers systematically studied functionalizing the peripheries of PAMAM and PPI dendrimers with salicylaldehyde moieties bearing one, two and three terminal aliphatic chains. From the studies, the authors identified that whereas the one terminal alkyl chain functionalized dendrimer generation exhibited varied lamellar smectic phases, two and three terminal aliphatic chain bearing dendrimers showed a hexagonal columnar mesophase. There were no differences in the mesophase structures of dendritic LCs arising from these two different types of dendrimer cores. Higher densities of aliphatic chains at the peripheries induced a curved and radial arrangement of the mesogenic moieties, leading to stacking of the molecules and formation of a columnar mesomorphism.⁴⁹ In another study, a hexagonal columnar mesomorphism was observed with third and fourth generation PPI and PAMAM dendrimers, peripherally functionalized with mesogenic groups. The functionalization of dendrimer with bulkier mesogenic group was performed with an aim to achieve cubic mesomorphism, however due to congestion of peripheral moieties, complete functionalization of dendrimer could not be achieved and a Colh

arrangement was observed for all the dendrimers, irrespective of the nature and generation of dendrimers and the promesogenic groups.⁵⁰

Importance of the spacer moiety connecting the peripheral mesogen with the dendritic core is studied in detail. Carbosilane dendrimers tethered directly with 36 and 108 cholesteryl groups, without a spacer moiety, do not show a mesogenic behavior,⁵¹ whereas similar carbosilane dendrimers possessing cyanobiphenyl moieties connected with the aid of undecyl chain exhibit generation-dependent mesophase behavior. Thus, dendrimer generations 1–4 remain to be smectic A and C mesogens, that of the fifth generation turns out to be not only lamellar, but also columnar mesophase structure, due to crowding of the mesogenic groups and the attendant spherical shape of the molecule.⁵²

Formation of smectic phase is seen prominently in PPI dendrimers attached with 4, 8, and 16 cholesteryl carbamate moiety at the peripheries of first, second and third generations, as a result of nanophase segregation of incompatible dendritic core and peripheral segments in these dendritic LCs.⁵³

Nanophase segregation of the dendritic core from the peripheral mesogenic groups is suggested as rationale for the observation of columnar mesophases in PPI dendrimers functionalized with 4, 8, 16, 32, and 64 peripheral triphenylene moieties, having a decylene spacer, in the first to fifth generations, respectively. Whereas the first generation dendritic LC showed a rectangular columnar arrangement, the remaining dendritic LCs possessed a hexagonal columnar arrangement.⁵⁴

Synthesis and phase behavior studies of carbosilane dendrimers functionalized with butoxyphenylbenzoate groups at the peripheries of first to five generations were studied by Agina and coworkers. Whereas first to fourth generation dendrimers possessing 8, 16, 32, and 64 mesogen moieties at the peripheries exhibited a lamellar phase (smectic C phase) that of the fifth generation dendrimer installed with 124 peripheral mesogen moiety showed supramolecular columnar structures. A microphase segregation of alternating dendritic core and the mesogenic moieties constituted the layer in the lamellar phase, whereas the whole molecule served as a structural unit in the case of the columnar phase. Further, the lamellar spacing increased with increasing temperature in all four generations, due to dendritic core assuming an isotropic conformation at higher temperature and overcome the interaction of mesogenic segments. Small angle neutron scattering studies further reiterated the observations from XRD studies.^{22b} Similar LC behavior was also observed to the series of carbosilane dendrimers functionalized with azobenzene mesogens linked through decylene chains.^{22a}

A long spacer is critical in order to make the peripheral mesogenic moieties independent of the influence of the dendritic core, to derive a stable mesophase structure.^{22a,55}

A series of homolithic and heterolithic eight-armed dendritic liquid crystals, in which either identical anisotropic segments

or different anisotropic segments form the branching cells with double multiplicity, respectively, was studied for their mesogenic properties by Donnio and coworkers.⁵⁶ Both the series showed either a lamellar or a columnar mesophase structures. Eight-armed dendrimers possessing one terminal alkyloxy chains at the peripheral aromatic moieties exhibited a lamellar phase, whereas incorporation of second alkyloxy chains at the same peripheral aromatic moieties led to the formation of a columnar phase. Incorporation of additional alkyl chain appeared to prevent parallel orientation of the mesogen moieties rather a radial arrangement around the dendritic core occurred, leading to column formation.⁵⁶

From a series of above studies and developments in dendritic liquid crystals, it becomes apparent that steric crowding is an important feature in those derivatives that show columnar mesophases. A steric crowding results frequently in a higher generation dendrimer, wherein the space and volume available to each peripheral mesogen-inducing moieties become progressively less, when compared to lower generation dendrimers. Second type of steric crowding at the peripheries are those derivatives in which more than one substituents, such as, long alkyl chains are installed at the outer-most moieties, primarily aromatic moieties. In these instances, locating one versus two or three long chain substituents leads to lamellar or columnar mesophase structures. Separation of peripheral mesogen-inducing moieties from the dendritic core with the of spacers is critical, absence of spacers renders the derivatives nonmesogenic.

This work illustrates the role of connectors, between aliphatic versus aromatic or ester versus amide connecting the dendrimer peripheries with the mesogenic units in identical dendrimer generations. Presence of succinate, succinamide, and phthalate ester connectors connecting the dendrimers with cholesterol provided a lesser volume fraction of dendrimers for phthalate ester connector in comparison to succinate ester and amide connectors within each generation, without changing the number of mesogenic moieties and the dendrimer generations. In addition to reduced volume fractions, extended rigidity and ortho-disubstitution in the structure of the mesogenic group facilitated the formation of two-dimensional rectangular columnar mesophase in the case of phthalate ester-connected third generation dendritic liquid crystal. It is thus inferred that the connectors connecting the dendritic core with peripheral mesogenic moieties play an important role in the molecular packing in the mesophase structures, even when the underlying dendritic core structures do not change. We premise that this observation is similar to that reported by Belaisaoui et al. wherein variations of mesophase structures were related to branching sugar moieties at the outer shell and very little or none of the effect arising due to the dendritic core sugar moiety.⁵⁷

CONCLUSIONS

In summary, the first, second and third generation amine and hydroxyl groups terminated PETIM dendrimers functionalized with cholesteryl moieties having succinate, succinamide, and

phthalate connectors were synthesized and their liquid crystalline (LC) properties were investigated through POM, DSC, and powder XRD analyses. The series of experiments demonstrated that LC dendrimers showed enantiotropic mesophase property. All the dendritic liquid crystals showed lamellar arrangement, except phthalate ester-linked **G3OCP₁₆**, which showed a two-dimensional rectangular columnar arrangement. The observed smectic phase of the dendritic LCs results from the dendritic core adopting topological changes as enforced by peripheral structurally rigid mesogenic segments and the flexible dendritic core. An introduction of the rigidity in the connectors, structure without changing its length from succinic to phthalic moieties showed a switch from smectic to two-dimensional non-centered rectangular columnar mesophase at the third generation, whereas first and second generation dendrimers showed smectic mesophase irrespective of their ester or amide connectors in their molecular structures. This study demonstrates a correlation between the connectors that connect the dendritic core with the peripheral mesogenic moieties and the resulting mesophase structures in dendritic liquid crystals, within a particular dendrimer generation, having identical underlying dendrimer core structures.

EXPERIMENTAL

Materials

Chemicals were purchased from commercial sources and were used without further purification. Solvents were dried and distilled using literature procedures. Triethylamine was stored over KOH. Analytical TLC was performed on commercial Merck plates, coated with silica gel 60 F₂₅₄ (0.25 mm) and aluminum oxide 60 F₂₅₄ (0.25 mm). Compounds were visualized by exposure to a UV lamp or incubation in a glass chamber containing iodine. Compounds were purified by column chromatography using neutral aluminum oxide and silica gel (100–200 mesh, SRL, India). **G1OCS₄** and **G2OCS₈** were prepared as described previously.¹⁹ FTIR spectra were recorded on a Perkin-Elmer spectrometer, as neat samples. ¹H and ¹³C NMR spectral analyses were performed on a Bruker-ARX400 operating at 400 and 100 MHz, respectively. Chemical shifts are reported with respect to tetramethylsilane (TMS) for ¹H NMR and the central line (77.0 ppm) of CDCl₃ for ¹³C NMR. Chemical shift values are reported in ppm relative to TMS and the following abbreviations are used to explain the multiplicities: s, singlet; d, doublet; t, triplet; q, quartet; m, multiplet; br, broad; dd, double doublet. Coupling constant (*J*) are reported in Hertz (Hz). Microanalysis was performed on an automated Carlo-Erba C, H, and N analyzer. High resolution mass spectra were obtained from a Micromass Q-TOF instrument by an electrospray ionization technique.

Synthesis of Cholesteryl Hydrogenphthalate

Triethyl amine (1.3 g, 12.9 mmol) and phthalic anhydride (1.92 g, 12.9 mmol) were added to a solution of cholesterol (5 g, 12.9 mmol) in CHCl₃ (50 mL). The solution was stirred at room temperature for 15 h. Progress of the reaction was monitored by TLC (SiO₂, I₂). After completion of the reaction,

chloroform (50 mL) was added to it. The organic layer was subsequently washed with aq. HCl (1 N) (2 x 50 mL), saturated NaHCO₃ (2 x 50 mL), brine solution (50 mL) and dried over anhydrous Na₂SO₄, followed by solvent evaporation *in vacuo*. The crude product was purified by column chromatography (SiO₂, 20% EtOAc-hexane) to afford **2**, as a white amorphous powder. Yield = 6.7 g (97%); *R_f* 0.5 (1:9 MeOH/CHCl₃); mp: 178.85 °C from DSC trace, second cycle; $[\alpha]_D^{20} = -36.02$ (*c* 1.00, CHCl₃); FTIR (neat): ν 2943, 1722, 1714, 1469, 1298, 1131, 1076, 946, 41 cm⁻¹; ¹H NMR (400 MHz, CDCl₃): δ 0.6–2.1 (m, 41 H, cholesteryl), 2.49 (m, 2 H, CH₂), 4.89 (m, 1 H, OCH), 5.43 (m, 1 H, CH), 7.58 (m, 2 H, CH), 7.71 (dd, *J*₁ = 7.6 Hz, *J*₂ = 1.2 Hz, 1 H, CH), 7.91 (dd, *J*₁ = 7.6 Hz, *J*₂ = 1.6 Hz, 1 H, CH); ¹³C NMR (100 MHz, CDCl₃): δ 171.8, 167.5, 139.4, 133.6, 132.0, 130.7, 129.9, 128.8, 122.9, 121.8, 75.8, 56.7, 56.1, 50.0, 42.2, 42.1, 39.7, 39.5, 37.8, 36.9, 36.6, 36.4, 36.1, 35.8, 31.8, 31.5, 28.2, 28.0, 27.7, 27.4, 24.2, 23.8, 22.8, 22.7, 22.5, 21.0, 19.3, 18.7, 11.8; HRMS: *m/z* C₃₅H₅₀O₄Na calcd. 557.3607, found 557.3608.

G3OCS₁₆

Oxalyl chloride (62 μ L, 0.74 mmol) was added to a solution of cholesteryl hemisuccinate (0.3 g, 0.62 mmol) in CH₂Cl₂ (5 mL), stirred for 10 min at 0 °C and then for 2 h at room temperature. Solvents were removed *in vacuo* and dried to afford cholesteryl hemisuccinate acid chloride. A solution of the acid chloride in CH₂Cl₂ (10 mL) was added to a solution of third generation hydroxyl group terminated PETIM dendrimer (0.063 g, 0.025 mmol), Et₃N (0.12 mL, 0.86 mmol), and DMAP (cat.) in CH₂Cl₂ (15 mL). The reaction mixture stirred at room temperature for ~10 h, diluted with CH₂Cl₂ (20 mL), washed with water (2 x 25 mL), the organic portion dried (Na₂SO₄), filtered, filtrate concentrated *in vacuo* and dried to afford a crude product. The crude product was triturated with n-hexane (25 mL), centrifuged, filtrate collected, evaporated *in vacuo*. The resulting residue was triturated again with n-hexane, centrifuged, filtrate collected and solvents evaporated *in vacuo*. The procedure was repeated 4 times, by which absence of insoluble cholesteryl hemisuccinic acid was ensured. The solvent was evaporated *in vacuo* and dried thoroughly to afford **G3OCS₁₆**, as a gummy solid. Yield: 0.23 g (90%); $[\alpha]_D^{20} = -25.4$ (*c* 1.00, CHCl₃). FTIR (neat) ν 2947, 1732, 1467, 1376, 1166, 760; ¹H NMR (400 MHz, CDCl₃): δ 0.5–2.10 (band, 772 H; cholesteryl, CH₂–CH₂–CH₂), 2.15–2.70 (br, 148 H, N–CH₂, –CH₂OCO–, –OCOCH₂), 3.32 (t, *J* = 5.8 Hz, 52 H, –CH₂–O–CH₂), 4.09 (t, *J* = 5.8 Hz, 32 H, CH₂COOCH–), 4.58 (br, 16 H, O–CH), 5.28 (br, 16 H, =CH); ¹³C NMR (100 MHz, CDCl₃): δ 172.3, 171.6, 139.5, 122.6, 74.2, 68.8, 62.9, 56.6, 56.0, 50.5, 50.2, 49.9, 42.2, 39.6, 39.4, 38.0, 36.9, 36.5, 36.1, 35.7, 31.8, 31.87, 29.4, 29.0, 28.2, 27.9, 27.7, 24.2, 23.8, 22.8, 22.5, 21.00, 19.3, 18.7, 11.8. Elemental analyses: calcd. for C₆₂₂H₁₀₃₆O₇₇N₁₄: C 75.14, H 10.50, N 1.97; found: C 75.15, H 10.31, N 2.44.

G1OCP₄

Oxalyl chloride (0.38 μ L, 0.45 mmol), a solution of cholesteryl hemiphthalate (0.22 g, 0.41 mmol) in CH₂Cl₂ (5 mL), first generation hydroxyl group terminated PETIM dendrimer

(0.03 g, 0.082 mmol), and Et₃N (0.075 mL, 0.54 mmol) in CHCl₃ (15 mL) and the reaction was proceeded further as given in the general method. Yield = 187 mg (97%); $[\alpha]_D^{20} = -34.80$ (*c* 1.00, CHCl₃); ¹H NMR (400 MHz, CDCl₃): δ 0.5–2.20 (br, 184 H, cholesteryl, CH₂–CH₂–CH₂), 2.43 (m, 12 H, CH₂NCH₂), 3.41 (m, 4 H, O–CH₂), 4.34 (br, 8 H, O–CH₂), 4.81 (br, 4 H, OCH), 5.39 (br, 4 H, =CH), 7.47 (br, 8 H, ArH), 7.64–7.71 (m, 8 H, ArH); ¹³C NMR (100 MHz, CDCl₃): δ 171.4, 167.5, 139.7, 139.4, 132.3, 132.1, 131.0, 130.9, 130.7, 130.2, 129.2, 128.9, 128.8, 128.5, 122.9, 122.7, 75.4, 75.2, 63.2, 56.7, 56.2, 50.0, 42.3, 39.7, 39.5, 38.0, 37.9, 37.0, 36.9, 36.5, 36.1, 35.8, 31.9, 31.8, 30.9, 29.9, 29.6, 29.3, 28.2, 27.9, 27.7, 24.2, 23.8, 22.8, 22.5, 21.00, 19.3, 18.7, 11.8; Elemental analysis. calcd for C₁₅₈H₂₃₂O₁₇N₂: C 78.04, H 9.62, N 1.15; found: C 77.92, H 9.35, N 1.35.

G2OCP₈

Oxalyl chloride (49 μL, 0.58 mmol), a solution of cholesteryl hemiphthalate (0.31 g, 0.58 mmol) in CH₂Cl₂ (5 mL), second generation hydroxyl group terminated PETIM dendrimer (0.061 g, 0.058 mmol), and Et₃N (0.096 mL, 0.69 mmol) in CHCl₃ (15 mL) and the reaction was proceeded further as given in the general method. Yield = 267 mg (94%); $[\alpha]_D^{20} = -30.60$ (*c* 1.00, CHCl₃); FTIR (neat): ν 3311, 2938, 2867, 1730, 1656, 1550, 1469, 1374, 1167, 1108 cm⁻¹; ¹H NMR (400 MHz, CDCl₃): δ 0.4–2.60 (br, 380 H, cholesteryl, –CH₂–), 2.79 (br, 20 H, CH₂), 3.32 (m, 20 H, CH₂OCH₂), 3.77 (br, 16 H, CH₂), 4.70 (br, 16 H, COOCH₂), 5.37 (br, 8 H, O–CH), 5.76 (br, 8 H, =CH), 7.73–8.08 (br, 32 H, ArH); ¹³C NMR (100 MHz, CDCl₃): δ 167.7, 140.7, 139.5, 139.4, 131.5, 130.9, 128.9, 122.5, 121.7, 75.6, 71.8, 60.3, 56.7, 56.2, 50.1, 50.0, 42.3, 42.2, 39.7, 39.5, 39.0, 37.8, 37.3, 36.9, 36.6, 36.5, 36.2, 35.8, 33.4, 31.9, 31.8, 31.7, 31.5, 29.7, 28.2, 28.0, 27.5, 24.3, 23.9, 22.8, 22.5, 21.0, 19.3, 18.7, 11.8; Elemental analysis. calcd for C₃₃₄H₅₀₀O₃₇N₆: C 77.27, H 9.71, N 1.62; found: C 77.05, H 9.61, N 1.41.

G3OCP₁₆

Oxalyl chloride (37 μL, 0.44 mmol), a solution of cholesteryl hemiphthalate (0.23 g, 0.43 mmol) in CH₂Cl₂ (5 mL), a solution of third generation hydroxyl group terminated PETIM dendrimer (0.053 g, 0.022 mmol), and Et₃N (0.067 mL, 0.48 mmol) in CH₂Cl₂ (15 mL). and the reaction was proceeded further as given in the general method. Yield = 0.21 g (92%); $[\alpha]_D^{20} = -27.6$ (*c* 1.00, CHCl₃). ¹H NMR (400 MHz, CDCl₃): δ 0.5–2.0 (band, 784 H, cholesteryl, CH₂–CH₂–CH₂), 2.43 (m, 32 H, CH₂), 2.80–3.30 (br, 60 H, –CH₂–), 3.39 (m, 32 H, –CH₂–O–CH₂), 3.60 (m, 16 H, NCH₂), 4.33 (br, 16 H, O–CH₂), 4.77 (br, 16 H, O–CH), 5.36 (br, 16 H, =CH), 7.35–7.70 (m, 64 H, ArH); ¹³C NMR (100 MHz, CDCl₃): δ 167.9, 139.7, 139.3, 131.7, 130.5, 128.9, 128.5, 128.1, 122.9, 122.5, 74.8, 56.6, 56.1, 49.9, 42.2, 39.6, 39.4, 37.9, 36.6, 36.1, 35.7, 31.9, 31.7, 28.1, 27.9, 24.2, 23.8, 22.7, 22.5, 21.0, 19.3, 18.7, 11.9; Elemental analysis calcd. for C₆₈₆H₁₀₃₆O₇₇N₁₄: C 76.92, H 9.75, N 1.83; found: C 77.02, H 9.54, N 1.61.

G1NHCS₄

Oxalyl chloride (46 μL, 0.54 mmol), a solution of cholesteryl hemisuccinate (0.22 g, 0.45 mmol) in CH₂Cl₂ (5 mL), first generation amine terminated PETIM dendrimer (0.053 g, 0.089 mmol), and Et₃N (0.090 mL, 0.65 mmol) in CHCl₃ (15 mL) and the reaction was proceeded further as described in the synthesis of G3OCS₁₆. Yield = 0.22 g (98%); $[\alpha]_D^{20} = -28.40$ (*c* 1.00, CHCl₃); FTIR (neat): ν 3310, 2933, 2868, 1729, 1650, 1552, 1469, 1374, 1170, 1111; ¹H NMR (400 MHz, CDCl₃): δ 0.5–2.1 (br, 184 H, cholesteryl, CH₂–CH₂–CH₂), 2.30 (m, 8 H, CH₂), 2.45 (m, 12 H, CH₂), 2.62 (m, 16 H, CH₂), 3.32 (m, 8 H, NH–CH₂), 3.45 (m, 20 H, O–CH₂), 4.60 (br, 4 H, O–CH), 5.35 (br, 4 H, =CH), 6.6 (br, 4 H, NH); ¹³C NMR (100 MHz, CDCl₃): δ 172.4, 171.7, 139.6, 122.5, 74.2, 69.0, 68.7, 56.7, 56.1, 50.0, 42.3, 39.7, 39.5, 38.0, 37.1, 36.9, 36.5, 36.1, 35.8, 31.9, 31.8, 30.9, 29.9, 29.6, 29.3, 28.2, 27.9, 27.7, 24.2, 23.8, 22.8, 22.5, 21.00, 19.3, 18.7, 11.8; Elemental analysis. calcd for C₁₅₄H₂₆₀O₁₇N₆: C 74.95, H 10.62, N 3.41; found: C 74.94, H 10.51, N 3.26.

G2NHCS₈

Oxalyl chloride (40 μL, 0.46 mmol), a solution of cholesteryl hemisuccinate (0.185 g, 0.38 mmol) in CH₂Cl₂ (5 mL), second generation amine terminated PETIM dendrimer (0.057 g, 0.038 mmol) and Et₃N (0.070 mL, 0.50 mmol) in CHCl₃ (15 mL) and the reaction was proceeded further as described in the synthesis of G3OCS₁₆. Yield = 0.19 g (95%); $[\alpha]_D^{20} = -29.80$ (*c* 1.00, CHCl₃); FTIR (neat): ν 3311, 2938, 2867, 1730, 1656, 1550, 1469, 1374, 1167, 1108 cm⁻¹; ¹H NMR (400 MHz, CDCl₃): δ 0.5–2.0 (br, 380 H, cholesteryl, CH₂–CH₂–CH₂), 2.10–2.80 (m, 84 H, CH₂), 3.32 (m, 16 H, NH–CH₂), 3.45 (m, 52 H, O–CH₂), 4.60 (br, 8 H, O–CH), 5.35 (br, 8 H, =CH), 6.6 (br, 8 H, NH); ¹³C NMR (100 MHz, CDCl₃): δ 172.4, 171.7, 139.7, 122.6, 74.2, 74.0, 68.7, 68.3, 56.7, 56.2, 50.0, 42.3, 39.7, 39.5, 38.0, 37.1, 36.9, 36.6, 36.2, 35.8, 31.9, 31.8, 30.9, 30.3, 29.9, 29.4, 28.2, 28.0, 27.7, 27.2, 26.2, 25.2, 24.3, 23.9, 22.8, 22.5, 21.0, 19.3, 18.7, 11.8; Elemental analysis. calcd for C₃₂₆H₅₅₆O₃₇N₁₄: C 74.38, H 10.65, N 3.73; found: C 74.28, H 10.55, N 3.56.

G3NHCS₁₆

Oxalyl chloride (40 μL, 0.47 mmol), a solution of cholesteryl hemisuccinate (0.19 g, 0.39 mmol) in CH₂Cl₂ (5 mL), a solution of third generation amine terminated PETIM dendrimer (0.065 g, 0.019 mmol), and Et₃N (0.070 mL, 0.5 mmol) in CH₂Cl₂ (15 mL) and the reaction was proceeded further as described in the synthesis of G3OCS₁₆. Yield 0.21 g (95%); $[\alpha]_D^{20} = -26.46$ (*c* 1.00, CHCl₃). FTIR (neat): ν 3317, 2938, 2856, 1732, 1653, 1563, 1464, 1375, 1256, 1174, 1120; ¹H NMR (400 MHz, CDCl₃): δ 0.5–2.1 (band, 772 H, cholesteryl, CH₂–CH₂–CH₂), 2.20–2.70 (m, 180 H, CH₂–CH₂–CH₂NH, N–CH₂, CO–CH₂–CH₂–CO), 3.32 (m, 32 H, NH–CH₂), 3.45 (m, 116 H, –CH₂–O–CH₂), 4.60 (br, 16 H, O–CH), 5.35 (br, 16 H, =CH), 6.4 (br, 16 H, NH); ¹³C NMR (100 MHz, CDCl₃): δ 172.4, 171.4, 139.7, 122.7, 74.3, 69.3, 56.7, 56.2, 50.9, 50.8, 50.0, 42.3, 39.8, 39.5, 38.1, 37.8, 37.0, 36.6, 36.2, 35.8, 31.9, 31.6, 31.4, 31.0, 30.5, 30.2, 29.9, 29.7, 29.5, 29.3, 29.1, 28.2, 28.0, 27.8, 27.6, 27.5, 26.2, 24.3, 23.9, 22.8, 22.6, 22.5, 21.0,

19.3, 18.7, 14.1, 11.9. Elemental analysis calcd. for $C_{670}H_{1148}O_{77}N_{30}$: C 74.12, H 10.66, N 3.87; found: C 74.31, H 10.46, N 3.59.

Instrumentation

The mesophase was characterized on untreated glass plate using a POM fitted with a hot stage. The transition temperatures and enthalpies were determined by DSC with nitrogen purging at a heating-cooling rate of $10\text{ }^{\circ}\text{C min}^{-1}$ for three cycles. From the second cycle, the maxima of the peaks were taken as transition temperatures and the mid-point of the heat capacity change were taken as glass transition temperature. Variable-temperature powder XRD studies were carried out with samples filled in Lindemann capillaries. The apparatus essentially involved a high-resolution X-ray powder diffractometer (PANalytical X'Pert PRO) with a high-resolution fast detector PIXCEL.⁵⁸

ACKNOWLEDGMENTS

The authors are grateful to Department of Science and Technology, New Delhi, for a financial support of the work. P. Kumar acknowledges Council of Scientific and Industrial Research, New Delhi, for a research fellowship.

REFERENCES AND NOTES

- J.-M. Lehn, *Supramolecular Chemistry: Concepts and Perspectives*; Wiley-VCH: Weinheim, **1995**.
- K. Ariga, T. Kunitake, *Supramolecular Chemistry - Fundamentals and Applications*; Springer-Verlag: Berlin, **2006**.
- B. M. Rosen, C. J. Wilson, D. A. Wilson, M. Peterca, M. R. Imam, V. Percec, *Chem. Rev.* **2009**, *109*, 6275.
- C. Tschierske, *J. Mater. Chem.* **2001**, *11*, 2647.
- G. R. Newkome, C. Shreiner, *Chem. Rev.* **2010**, *110*, 6338.
- A.-M. Caminade, C. O. Turrin, R. Laurent, A. Quali, B. D. Nicot, *Dendrimer: Towards Catalytic, Material and Biomedical Uses*; Wiley-VCH: Weinheim, **2011**.
- N. E. Domracheva, V. I. Morozov, M. S. Gruzdev, R. A. Manapov, A. V. Pyataev, G. Lattermann, *Macromol. Chem. Phys.* **2010**, *211*, 791.
- A. Yoshizawa, *Polym. J.* **2012**, *44*, 490.
- M. Marcos, R. Martín-Rapún, A. Omenat, J. L. Serrano, *Chem. Soc. Rev.* **2007**, *36*, 1889.
- M. Yoshio, R. Konishi, T. Sakamoto, T. Kato, *New J. Chem.* **2013**, *37*, 143.
- B. Donnio, S. Buathong, I. Bury, D. Guillon, *Chem. Soc. Rev.* **2007**, *36*, 1495.
- S. Hernandez-Ainsa, E. Fedeli, J. Barbera, M. Marcos, T. Sierra, J. L. Serrano, *Soft Matter.* **2014**, *10*, 281.
- J. D. Barrio, R. M. Tejedor, L. S. Chinelatto, C. Sánchez, M. Piñol, L. Oriol, *Chem. Mater.* **2010**, *22*, 1714.
- T. Felekis, D. Tsiourvas, L. Tziveleka, C. M. Paleos, *Liq. Cryst.* **2005**, *32*, 39.
- O. Haba, D. Hiratsuke, T. Shiraiwa, T. Koda, K. Yonetake, Y. Momoi, K. Furuta, *Mol. Cryst. Liq. Cryst.* **2013**, *574*, 84.
- A. Bobrovsky, N. I. Boiko, V. Shibaev, *Polymer.* **2015**, *56*, 263.
- J. Sun, Y. Lin, *J. Polym. Sci. Part A: Polym. Chem.* **2013**, *51*, 71.
- L. L. Lai, J. W. Hsieh, K. L. Cheng, S. H. Liu, J. J. Lee, H.F. Hsu, *Chem. Eur. J.* **2014**, *20*, 5160.
- P. Kumar, D. S. S. Rao, S. K. Prasad, N. Jayaraman, *Polymer.* **2016**, *86*, 98.
- B. Donnio, D. Guillon, *Adv. Polym. Sci.* **2006**, *201*, 45–155.
- S. Ferin, F. Cameral, R. Ziessel, J. Barberá, R. Deschenaux, *Chem. Mater.* **2009**, *21*, 3950.
- (a) B. I. Ostrovskii, S. N. Sulyanov, N. I. Boiko, V. P. Shibaev, S. B. Astafev, L. G. Yanusova, W. H. de Jeu, *Eur. Phys. J. E.* **2013**, *36*, 134; (b) E. V. Agina, N. I. Boiko, R. M. Richardson, B. I. Ostrovskii, V. P. Shibaev, E. A. Rebrov, A. M. Muzafarov, *Polym. Sci. Ser. A* **2007**, *49*, 412.
- R. Martín-Rapún, M. Marcos, A. Omenat, J. Barberá, P. Ramero, J. L. Serrano, *J. Am. Chem. Soc.* **2005**, *127*, 7397.
- (a) S. A. Ponomarenko, E. A. Rebrov, A. Y. Bobrovsky, N. I. Boiko, A. M. Muzafarov, V. P. Shibaev, *Liq. Cryst.* **2006**, *33*, 1497; (b) N. I. Boiko, I. D. Leshchiner, E. V. Agina, R. Richardson, V. P. Shibaev, *Polym. Sci. Ser. A* **2011**, *53*, 645.
- O. Haba, K.-I. Okuyama, H. Osawa, K. Yonetake, *Liq. Cryst.* **2005**, *32*, 633.
- M. W. P. L. Baars, S. H. M. Söntjens, H. M. Fischer, H. W. I. Peerlings, E. W. Meijer, *Chem. Eur. J.* **1998**, *4*, 2256.
- L. Pastor, J. Barbera, M. McKenna, M. Marcos, R. Martín-Rapún, J. L. Serrano, G. R. Luckhurst, A. Mainal, *Macromolecules.* **2004**, *37*, 9386.
- (a) R. Elsäuer, G. H. Mehl, J. W. Goodby, M. Veith, *Angew. Chem. Int. Ed.* **2001**, *40*, 2688–2690; (b) I. M. Saez, J. W. Goodby, *Chem. Eur. J.* **2003**, *9*, 4869.
- B. Donnio, J. Barberá, R. Giménez, D. Guillon, M. Marcos, J. L. Serrano, *Macromolecules.* **2002**, *35*, 370.
- L. Gehringer, C. Bourgogne, D. Guillon, B. Donnio, *J. Mater. Chem.* **2005**, *15*, 1696.
- (a) T. R. Krishna, N. Jayaraman, *J. Org. Chem.* **2003**, *68*, 9694; (b) G. Jayamurugan, N. Jayaraman, *Tetrahedron* **2006**, *62*, 9582.
- I. Dierking, *Textures of Liquid Crystals*; Wiley-VCH: Weinheim, **2003**.
- C. Jana, G. Jayamurugan, R. Ganapathy, P. K. Maiti, N. Jayaraman, A. K. Sood, *J. Chem. Phys.* **2006**, *124*, 204719.
- J.-M. Rueff, J. Barberá, B. Donnio, D. Guillon, M. Marcos, J. L. Serrano, *Macromolecules.* **2003**, *36*, 8368.
- B. M. Craven, G. T. DeTitta, *J. Chem. Soc. Perkin Trans.* **1976**, *2*, 814.
- A.-M. Levelut, *J. Phys. Lett.* **1984**, *45*, L-603.
- See for example: *Liquid Crystals Materials Design and Self-Assembly*; C. Tschierske, Ed.; Springer-Verlag: Berlin, **2012**; pp 41.
- B. Soberats, M. Yoshio, T. Ichikawa, X. Zeng, H. Ohno, G. Ungar, T. Kato, *J. Am. Chem. Soc.* **2015**, *137*, 13212.
- T. Sakurai, Y. Tsutsui, K. Kato, M. Takata, S. Seki, *J. Mater. Chem. C* **2016**, *4*, 1490.
- K. Tanabe, T. Yasuda, M. Yoshio, T. Kato, *Org. Lett.* **2007**, *9*, 4271.
- K. Kishikawa, S. Nakahara, Y. Nishikawa, S. Kohmoto, M. Yamamoto, *J. Am. Chem. Soc.* **2005**, *127*, 2565.
- S. Hernandez-Ainsa, J. Barberá, M. Marcos, J. L. Serrano, *Soft Matter.* **2011**, *7*, 2560.
- A. van-Quynh, D. Filip, C. Cruz, P. J. Sebastião, A. C. Ribeiro, J.-M. Rueff, M. Marcos, J. L. Serrano, *Eur. Phys. J. E.* **2005**, *18*, 149.
- L.-L. Lai, S.-J. Hsu, H.-C. Hsu, S.-W. Wang, K.-L. Cheng, C.-J. Chen, T.-H. Wang, H.-F. Hsu, *Chem. Eur. J.* **2012**, *18*, 6542.

- 45** K. Lorenz, H. Frey, B. Stühn, R. Mulhaupt, *Macromolecules*. **1997**, *30*, 6860.
- 46** M. W. P. L. Baars, S. H. M. Söntjens, H. M. Fischer, H. W. I. Peerlings, E. W. Meijer, *Chem. Eur. J.* **1998**, *4*, 2456.
- 47** K. Yonetake, T. Masuko, T. Morishita, K. Suzuki, M. Ueda, R. Nagahata, *Macromolecules*. **1999**, *32*, 6578.
- 48** (a) J. Barbéra, A. C. Garcés, N. Jayaraman, A. Omenat, J. L. Serrano, J. F. Stoddart, *Polym. Prep. Am. Chem. Soc. Div. Polym. Chem.* **1999**, *40*, 488; (b) J. Barbéra, A. C. Garcés, N. Jayaraman, A. Omenat, J. L. Serrano, J. F. Stoddart, *Adv. Mater.* **2001**, *13*, 175.
- 49** M. Marcos, R. Giménez, J. L. Serrano, B. Donnio, B. Heinrich, D. Guillon, *Chem. Eur. J.* **2001**, *7*, 1006.
- 50** J.-M. Rueff, J. Barberá, M. Marcos, A. Omenat, R. Martín-Rapún, B. Donnio, D. Guillon, J. L. Serrano, *Chem. Mater.* **2006**, *18*, 249.
- 51** K. Lorenz, D. Hölter, H. Frey, B. Stühn, *Polym. Mater. Sci. Eng.* **1997**, *77*, 168.
- 52** S. A. Ponomarenko, N. I. Boiko, V. P. Shibaev, R. M. Richardson, I. J. Whitehouse, E. A. Rebrov, A. M. Muzafarov, *Macromolecules*. **2000**, *33*, 5549.
- 53** D. Tsiourvas, T. Felekis, Z. Sideratou, C. M. Paleos, *Macromolecules*. **2002**, *35*, 6466.
- 54** M. D. McKenna, J. Barberá, M. Marcos, J. L. Serrano, *J. Am. Chem. Soc.* **2005**, *127*, 619.
- 55** R. Martín-Rapún, M. Marcos, A. Omenat, J.-L. Serrano, G. R. Luckhurst, A. Mainal, *Chem. Mater.* **2004**, *16*, 4969.
- 56** (a) L. Gehringer, C. Bourgogne, D. Guillon, B. Donnio, *J. Am. Chem. Soc.* **2004**, *126*, 3856; (b) J. Wolska, J. Mieczkowski, D. Pocięcha, S. Buathong, B. Donnio, D. Guillon, E. Gorecka, *Macromolecules*. **2009**, *42*, 6375.
- 57** A. Belaisaoui, I. M. Saez, S. J. Cowling, J. W. Goodby, *Macromolecules*. **2013**, *46*, 1268.
- 58** D. S. Shankar Rao, M. Vijay Kumar, S. Krishna Prasad, U. S. Hiremath, M. Sarvamangala, S. Basavaraja, *J. Mater. Chem. C*. **2013**, *1*, 7488.